# Optical diagnostic techniques in ophthalmology

de Kinkelder, R.

**Publication date**
2012

# CHAPTER TWO

## COMPARISON OF RETINAL NERVE FIBER LAYER THICKNESS MEASUREMENTS BY SPECTRAL-DOMAIN OPTICAL COHERENCE TOMOGRAPHY SYSTEMS USING A PHANTOM EYE MODEL


### Abstract

To quantify differences in nerve fiber layer thickness measurements by various spectral-domain optical coherence tomography (SD-OCT) systems, we developed a phantom eye model. We tested twelve SD-OCT systems of four manufacturers. All systems combined overestimated the 49 µm thick phantom RNFL thickness on average by 18 µm. Within brands, thickness measurements differed statistically significant for one Topcon, one RTVue and one Cirrus. Between brands, thickness determined with RTVue and Topcon differed statistically significant from Cirrus and Spectralis. The maximum difference between mean thicknesses is 3.6 µm within brands and 7.7 µm between brands.



**This chapter is published in:**
***Journal of Biophotonics*** **(2012)**



**R. de Kinkelder**, D.M. de Bruin, F.D. Verbraak, T.G. van Leeuwen, D.J. Faber


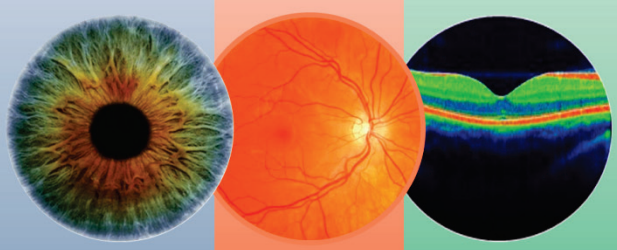

## 2.1 INTRODUCTION

In ophthalmology, optical coherence tomography (OCT) (1) is mainly used for imaging the central retina, to monitor the retina-vitreous interface, sub- and intra-macular edema (2) and for measuring the retinal thickness (3). Accurate determination of the thickness of the retinal nerve fiber layer (RNFL) around the optic nerve is important for diagnosis and follow-up of glaucoma patients (3, 4). Recently, several spectral domain OCT (SD-OCT) systems have become commercially available that allow calculation of thickness maps around the optic nerve and the macula within a couple of seconds. Although most systems provide a protocol to determine the RNFL thickness in a circular scan around the optic nerve with a fixed diameter of 3.4 mm, direct comparison of RNFL thickness measurements with different OCT devices measuring human eyes is complicated because the true RNFL thickness is unknown. Within one subject, spatial variations in thickness can induce differences in RNFL thickness measurements, e.g. when the position of the circular scan around the optic nerve is not the same or when the tested subject is fixating at another location.

Various studies have addressed the challenge to determine the repeatability of RNFL thickness measurements of TD-OCT (5) and SD-OCT systems (6-11) using human subjects, requiring large populations and multiple measurements on each subject. A study by Leite *et al*. showed differences between various OCT systems when measuring the RNFL thickness up to 40 μm in one population (6), which exceeded the axial resolution of most systems (in the order of 5-10 μm). They conclude that the used protocol in that study, a circular scan around the optic nerve, caused large fluctuations in the calculated RNFL thickness due to the inhomogeneity of the tissue morphology, which hampered quantitative comparison between the devices.

Therefore, comparison using device independent, reproducible samples that mimic the relevant tissue geometry is highly preferable. Moreover, using a phantom with known layer thickness easily allows re-evaluation of the responses, for example after servicing or manufacturer software updates.

We developed a phantom eye model containing a silicone based phantom retina of five layers with various scattering properties (12). Using this eye model, we quantified the intra-brand and inter-brand variation of RNFL thickness measurements for four brands of SD-OCT devices.

## 2.2 MATERIALS AND METHODS

### *2.2.1 PHANTOM EYE MODEL*

The phantom eye model (see Figure 2-1A) consisted of a container (I) that was filled with water to represent the vitreous. An achromatic lens (Edmund Optics; NT47-692; f = 20mm) was positioned at the front side of the container (II), mimicking the cornea and lens of the eye. A silicone based phantom retina was placed inside a concave, hemispherical holder (VI) that was positioned inside the container. The phantom retina was aligned in the focus of the lens using a translation stage (III). Changing this position mimics ametropia. To mimic cataract or other disturbances of the eye, a filter can be placed in front of the phantom retina using a filter mount (V). A transparent cover (IV) was positioned on top of the phantom eye. In figure 1B, the phantom eye was positioned on top of a variable friction arm (Manfrotto+Co., 244N, Italy) to ensure equal alignment between various OCT devices.

### *2.2.2 THE PHANTOM RETINA*

The phantom retina was based on thin layered silicone tissue phantoms stacked on top of each other, which were previously reported by De Bruin [12] *et al*. In brief, silicone (Sylgard 184, silicone elastomer, DOW/Corning) is a hydrophobic, two-component product (curing agent and silicone) with a refractive index of 1.41.

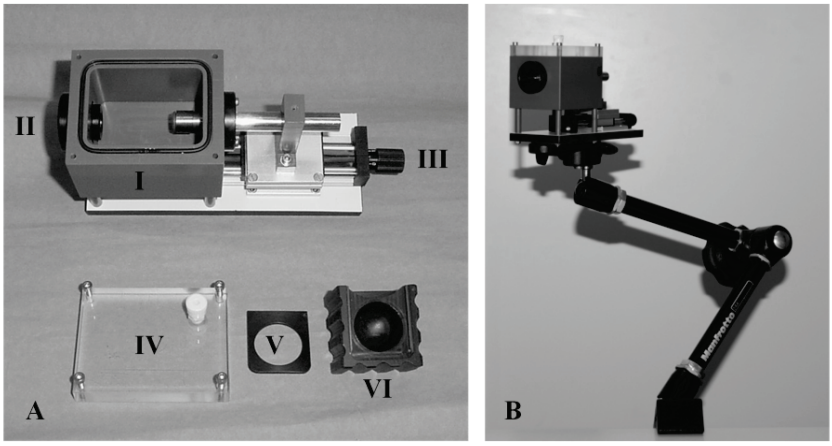


**Figure 2-1**: A: The parts of the eye model are displayed separately. A container (I) in which the phantom retina (VI) is positioned contains water and an achromatic lens, f=20mm (II). The retina can be put in focus by a translation stage (III). The cover (IV) is used to close the eye model. For the use of filters a filter holder (V) can be positioned in front of the retina. B: To enable alignment of the phantom eye model, it was positioned on a variable friction arm.

The scattering properties of the silicone based phantom layers are determined by the refractive index mismatch between the silicone and curing agent matrix and suspended particles. To vary the scattering coefficients of the layers we used different concentrations of titanium dioxide (TiO2) powder. Optical properties of the elastomer can be varied using different concentration of particles and the optical properties were shown to be constant over a prolonged period of time (12). For each layer the desired concentration of scatterers was mixed with the curing agent of the silicone elastomer. Homogeneous mixture was obtained using a tissue homogenizer with a small spacing between tube and pillar. The mixture was mixed with silicone under careful stirring using a standard laboratory mixer. Air bubbles were then removed with a vacuum pump, which kept the mixture under low pressure conditions. A small amount of the mixture was placed between two flat, heavy glass plates separated by placing brass foil with uniform thickness (50 μm) at the edges of the glass plate. The mixture was cured at 60 °C for 6 hours.

The phantom retina, displayed in Figure 2-2A, consisted of five non-light absorbing layers (10x10mm$^2$) with alternating light scattering properties (13, 14). Table 2-1 shows the scattering coefficients of the individual layers as measured previously with OCT at 830 nm (12) and average thickness of the layers as measured by a high precision caliper tool (5 separate measurements; also reported are the standard errors of the mean). Note that the contrast between layer I and II in our phantom retina is larger than the contrast between a real RNFL and the next-in-depth ganglion cell layer (GCL). We maximized contrast to ensure successful segmentation by the SD-OCT system.

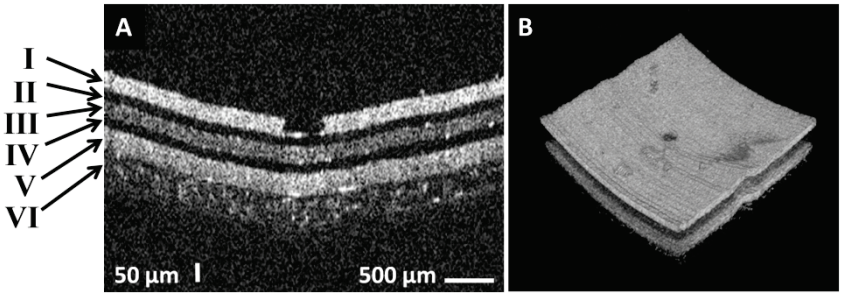


**Figure 2-2:** A cross-sectional image of the phantom retina made with Topcon 3DOCT-1000. The top layer (I thickness: 49 ± 1 μm, 0.5w% $TiO_2$ μt=11mm-1) mimics the RNFL. Layers II to V had a thickness of 63 μm, 53 μm, 63 μm, and 55 μm, respectively. The gap in the middle is used as fixation or marker during imaging. Total thickness of 5 layers = 283 ± 5 μm. The bottom layer is adhesive tape (VI).
B: 3D representation of the phantom retina acquired with Topcon 3DOCT-1000. The bottom and top layer (containing the hole in the middle) are clearly visible. The less scattering layer III is also visible in between the highly scattering layers. The dimensions of the phantom material are 6x6 mm.

**Table 2-1:** Optical properties of the layers in the phantom eye model and the geometrical thicknesses a measured with a high precision caliper

| Layer (see figure 2-2A) | OCT attenuation coefficient (see(12)) $\mu_t$ [mm-1] | Caliper thickness measurements | |
|---|---|---|---|
| | | Mean [µm] | Stand. Error [µm] |
| I | 11 | 49 | 0.2 |
| II | 0 | 63 | 0.5 |
| III | 2.1 | 53 | 0.2 |
| IV | 0 | 63 | 0.5 |
| V | 17 | 55 | 0.4 |

The five silicone layers were placed on top of each other and put in a vacuum chamber to remove air gaps between the layers. Electrostatic forces keep the layers together. The total geometrical thickness was 283±0.9 µm (layers I to V in Figure 2-2A) after stacking of the silicone layers of the phantom retina. The compound phantom is attached to the holder with adhesive tape (Layer VI in Figure 2-2). The top layer has a small hole in the center, which is used as fixation target during alignment to prevent tilting of the phantom eye in the OCT image.

### *2.2.3 OCT-SYSTEMS*

We evaluated SD-OCT systems of four manufacturers (RTVue by OptoVue, software version A4.0.5.100; 3DOCT-1000 by Topcon, software version v4.11; Cirrus by Zeiss Systems, software version 4.5.1.11; Spectralis by Heidelberg, software version 5.2.4.0). Three systems of each manufacturer were used to measure our phantom eye model, 5 times per device (which includes removing and repositioning the phantom eye model). The specified axial resolution of the systems, determining the precision of thickness measurements was ~5-10 µm. The lateral resolution, normally determined by the optics of the eye in case of human subjects, was 20 µm when imaging our phantom eye.

An average RNFL thickness was determined by the software of each apparatus using a circular scan (Ø=3.4mm) around a fixed location in the phantom eye (small hole in the top layer, see Figure 2-2). Since this scanning protocol was not directly available in the Cirrus software, we used the Optic Disc cube 200x200 module to image an area of approximately 6 x 6 mm. The Cirrus software computed an RNFL thickness map from this data. Subsequently, RNFL thicknesses were calculated at every clock hour on a circle (Ø=3.4 mm, placed by the operator on the thickness map). Finally, we averaged these clock hour values to obtain a single RNFL thickness for comparison with the other instruments.

All thickness measurements were corrected for the mismatch between the actual refractive index of silicone (n= 1.41) and the refractive index of tissue used by the

SD-OCT devices (n=1.35), i.e. which slightly reduced the values reported by the OCT system software. All segmented data was checked on segmentation artifacts e.g. due to small dust particles in the phantom construction process before the data was used for analysis.

### *2.2.4 STATISTICS*

A SPSS statistical software package (Version 16.0, Release 16.0.1; SPSS Inc., Chicago, IL, USA) was used for data analysis. The variation in RNFL thickness measurements within each device was expressed as standard deviation of five measurements. Furthermore, a coefficient of variance (COV) was calculated as the percentual ratio between the standard deviation and the average thickness. To compare the mean thickness measurements of the devices from one manufacturer we used ANOVA tests. The Levene statistic was calculated first to verify equality of the variances. A post hoc test was used to determine which device was significantly different. The variability between the manufacturers was determined using a univariate ANOVA test and post hoc test.

## 2.3 RESULTS

An OCT image of the developed phantom retina, obtained with Topcon 3DOCT-1000 is displayed in Figure 2-2A, and a three-dimensional representation is given in Figure 2-2B.

**Table 2-2:** The average thickness, standard deviation and coefficient of variance are shown for three devices of 4 different SD-OCT manufacturers that were measured 5 times.

| OCT device (Brand) | OCT device (#) | Average thickness [µm] | standard deviation [µm] | COV [%] |
|---|---|---|---|---|
| RTVue of Optovue (A) | 1 | 65.1 | 1.1 | 1.7 |
| | 2 | 66.1 | 1.5 | 2.7 |
| | 3 | 62.8 | 1.6 | 2.5 |
| | average | 64.7 | 2.0 | 3.1 |
| 3DOCT-1000 of Topcon (B) | 1 | 63.9 | 0.5 | 0.8 |
| | 2 | 66.8 | 1.0 | 1.5 |
| | 3 | 66.5 | 0.9 | 1.4 |
| | average | 66.1 | 1.8 | 2.8 |
| Cirrus of Zeiss (C) | 1 | 67.7 | 0.4 | 0.6 |
| | 2 | 70.5 | 0.9 | 1.3 |
| | 3 | 66.9 | 1.2 | 1.8 |
| | average | 68.4 | 1.7 | 2.4 |
| Spectralis of Heidelberg (D) | 1 | 69.0 | 0.6 | 0.9 |
| | 2 | 67.9 | 0.3 | 0.4 |
| | 3 | 68.3 | 2.0 | 2.9 |
| | average | 68.4 | 1.3 | 1.8 |

The average thickness, standard deviation and coefficient of variance are given in Table 2-2. We found low coefficients of variation for all systems ranging from 0.4% (for a Spectralis system) up to 2.9% (for a Spectralis system).

In Figure 2-3 the results of the five measurements per device of the various manufacturers are shown in box plots. Calculation of the Levene statistic *L* prior to ANOVA analysis showed that the variance in thickness measurements was not statistically different within brands (RTVue $L$= 0.455, p = 0.645; Topcon $L$ = 0.495, p = 0.621; Cirrus $L$ = 0.862, p=0.447; Spectralis $L$ = 3.545, p=0.062).

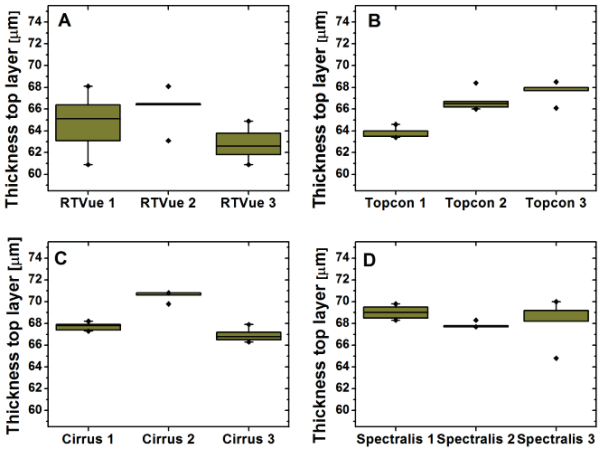


**Figure 2-3:** Thickness measurements of 3 OCT systems per brand measured 5 times using the phantom eye model. The bottom and top of the box plot (indicated with bars) display the 25th and 75th percentile of the data; the band around the median is the 50th percentile. The maximum and minimum thickness are indicated with ♦
A: RTVue of OptoVue
B: 3DOCT-1000 of Topcon.
C: Cirrus of Zeiss
D: Spectralis of Heidelberg

RTVue 3 shows a statistically significant lower average thickness ($F(2,12)=6.17$, $p=0.014$) with a maximum difference between the means of the other RTVue systems of 3.3 µm. The results of 3DOCT-1000 of Topcon are shown in Figure 2-3B. Topcon 1 differs statistically significant with the other two systems ($F(2,12)=29.113$, $p<0.001$), with a maximum difference between the means of 2.9 µm.

In Figure 2-3C, the results of Cirrus 2 differ statistically significant from the other two systems ($F(2,12)=74.788$, $p<0.001$), with a maximum difference between the means of 3.6 µm. In Figure 2-3D the results of the Spectralis measurements are shown. No statistically significant differences between the Spectralis devices are found ($F(2,12)=1.11$, $p=0.361$).

In Figure 2-4 the results of all measurements are displayed, categorized by manufacturer. The mean thicknesses measured using Topcon and OptoVue machines differ significantly from those obtained by Cirrus and Spectralis machines. Spectralis' intra-brand variability is smaller compared to the other manufacturers ($p<0.001$).

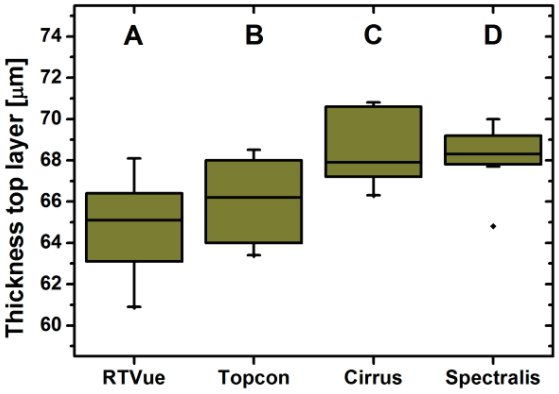


**Figure 2-4:** The results of 'RNFL' thickness measurements as calculated by the manufacturer's software are organized by manufacturer.

A: RTVue of OptoVue
B: 3DOCT-1000 of Topcon.
C: Cirrus of Zeiss
D: Spectralis of Heidelberg

## 2.4 DISCUSSION

We developed to our knowledge the first layered phantom eye model containing a silicone based phantom retina of five layers with various scattering properties for OCT thickness measurements. Scott Rowe *et al*. developed a retinal tissue phantom with uniform thickness of the layers down to 60 µm, however the model shows hardly any contrast between the layers and is therefore less suited for OCT thickness measurements (15). Other well calibrated eye models were designed for applications outside the field of OCT. For instance, Mordant *et al*. and Lemaillet *et al*. used an eye phantom for oximetry measurements in the retina (16, 17). Romero-Borja *et al*. used a spectralon based eye model to calibrate their adaptive optics scanning laser ophthalmoscope(18).

Introduction of new clinical (OCT) instruments requires demonstration of good repeatability and reproducibility as well as comparison of performance with respect to systems that are used in clinical practice. In this study we have compared RNFL thickness measurements between various clinically used SD-OCT devices and tested their repeatability using a phantom eye model representative of a healthy retina that contains thin silicone layers with controlled thickness and high scattering contrast between layers. We found minimal variation for the Spectralis systems (average COV: 1.8%) and highest for RTVue systems (average COV: 3.1%). The average COV of the Topcon and Cirrus systems are 2.8% and 2.4%, respectively. In three brands we observed one device that produced statistically significant different thickness values. The standard deviation of RTVue measurements is somewhat larger than those of other brands.

In clinical practice, following patients on different OCT devices is sometimes inevitable (e.g. after software upgrade, device replacement, transition of the patient

to or from other hospitals, etc). Our study shows that despite the statistically significant differences these patients can be reliably followed because of the high inter-brand (maximum difference 7.7 µm) and intra-brand (maximum difference 3.6 µm) reproducibility of the investigated systems. Please note that it is more important that the inter-brand difference is known instead of small when patients are measured on a different device from another brand.

None of the devices calculated the correct geometrical thickness of the top silicone layer of 49 µm. Averaged over all systems, 67 ± 4.0 µm was found (mean and standard deviation). This difference arises at least in part due to the unknown implementation of the segmentation algorithm(s) that is kept confidential by the manufacturers. To illustrate this, we show an averaged depth profile (64 A-scans) of our phantom retina in Figure 2-5.

The data was obtained with the Topcon 3DOCT-1000, the only system that allowed us direct access to the measured data. Surprisingly, when the thickness is determined between the maximums of phantoms front and back surface, the thickness (289 ± 10 µm) nearly matches the geometrical thickness (283 µm ± 10 µm). The 10 µm uncertainty estimates in the OCT data are based on the digital (pixel) resolution of the exported data.

The individual layer thicknesses are accurately retrieved using manual segmentation as illustrated in the figure. It is conceivable that the OCT systems' segmentation routines use more conservative estimates such as Full-Width at Half-Maximum, or the position of the largest gradient to determine layer thicknesses leading to larger reported thickness values. However, this effect is likely less pronounced in samples with lower contrast than between the layers in our phantom.

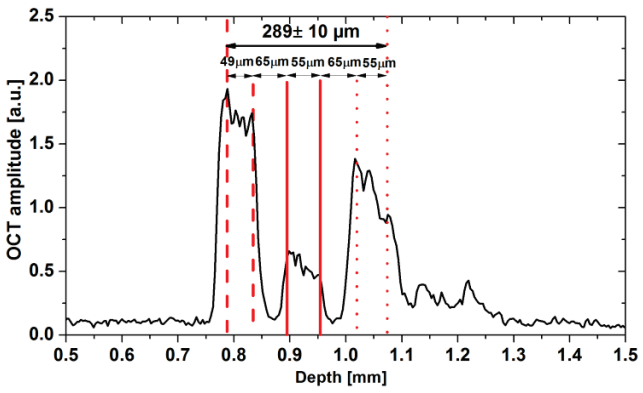


**Figure 2-5:** Average depth profile of the phantom retina measured with 3DOCT-1000 of Topcon. The thickness between the maximums at the layer transition matches the geometrical thickness of the phantom retina. The data is corrected for refractive index mismatch and shows the real, geometrical thickness.

Many factors can contribute to erroneous thickness measurements such as inadequate dispersion compensation or faulty k-calibration of the spectrometer (directly translating into the scaling of the depth axis (19)), but also specular reflection at the vitreo-retinal interface or broadening of response peak due to a finite optical resolution can contribute to erroneous thickness measurements.

To illustrate this we performed an OCT measurement on a glass slide (an averaged depth profile is given in Figure 2-6; averaged over 10 consecutive A-lines at the same location) with a thickness of 158 µm. The data is corrected for refractive index of glass (1.50).

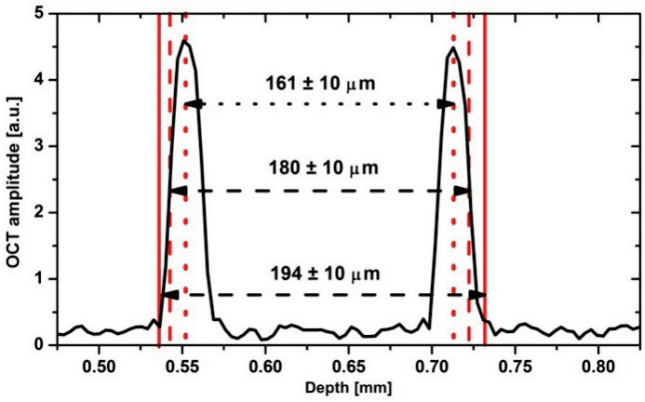


**Figure 2-6:** Average depth profile of a cover glass (158 µm) measured with 3DOCT-1000 of Topcon. Depending on the used algorithm the thickness of the glass is 194 ± 10 µm measured at full width, 180 ± 10 µm full widths half maximum and 161 ± 10 µm measured at the two maximums.

The figure shows two peaks indicating the air-glass and glass-air interface. The maximum value of the resulting OCT image determines the position of the interface assuming that the interfaces are delta response functions. In this case, the width of the peak at the glass-air interfaces represents the finite resolving power of the used OCT system. With decreasing resolution a broadening of this peak occurs that results in a thicker glass slide in case of a full width at half maximum segmentation criterion. The signal is adequately described as the convolution of the reflectance profile (two delta functions) with the envelope of the coherence function.

In the retina (and in the phantom), the interface between layers is better described by a step edge instead of a delta function. This reflectivity profile is convolved with the point spread function of the system, resulting in a degraded edge, e.g. resembling an error function. In this case, to accurately determine the position of the interface, one would look for the location of the largest gradient.

To correctly interpret these positions in relation to the actual thickness, the coherent nature of the PSF, e.g. the band-pass filtering property of OCT in the spatial frequency domain (20) needs to be taken into account. The incoherent (i.e.

envelope, dashed line in figure 1-6) point spread function is centered around zero-spatial frequencies (its width is the spectral bandwidth of the source). Such a measurement is thus sensitive to the lower frequency contributions of the samples' spectrum; i.e. it has low-pass filter characteristics. The coherent point spread function is centered around the source's central wave number and has band-pass filter characteristics. It is this latter point spread function that should be used when describing OCT signal formation.

Consider an idealized single-layer sample with reflectivity R($z$) = 1 within the layer, and R($z$) = 0 elsewhere, with $z$ being the position in depth and layer thickness exceeding the coherence length. Using the incoherent PSF, the lower spatial frequencies of the reflectivity profile can be recovered (whereas higher spatial frequencies cannot). In reality, when using the coherent point spread function, both the lower and higher spatial frequencies are not recovered, only a range of frequencies determined by the source spectrum. The OCT signal shows two *peaks*, located at the layer's interfaces (analogous to the image obtained from a glass slide, dotted line in figure 2-7). The specific appearance of the peaks depends on the range of spatial frequencies that is sampled, e.g. on the spectral bandwidth of the OCT system.

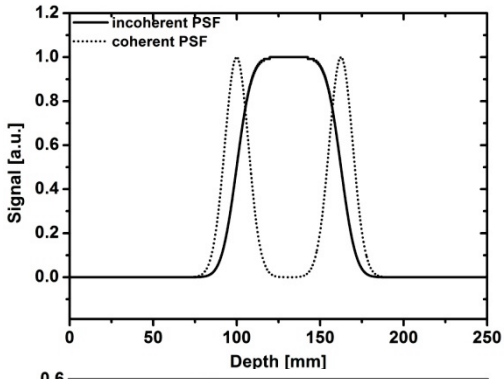


**Figure 2-7**: Convolution of the incoherent PSF with the simulated reflectivity profile shown as solid line and the coherent PSF as dotted line. The width of both PSF is 16.6 µm for this particular simulation.

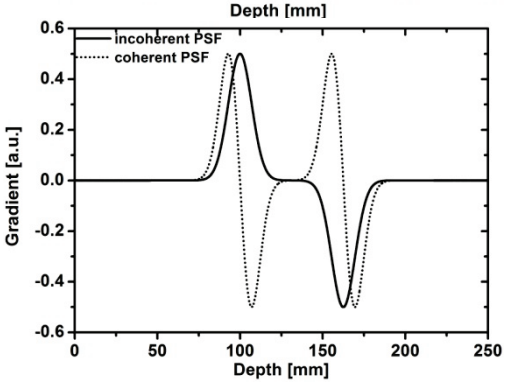


**Figure 2-8:** The gradient of the reflectivity profile from Figure 2-7 is displayed as a solid line for the incoherent PSF and as dotted line for the coherent PSF.

To illustrate the argument, we performed a pilot simulation as follows. A reflectivity profile of a numerical phantom is constructed by randomly placing a large number of delta-function reflectors within the layer's boundaries, with randomly chosen amplitude. We subsequently performed two analyses: we convolved the reflectivity profile with the incoherent and coherent PSF (see Figure 2-7, the width of both PSF is 16.6 μm to illustrate the difference). In the latter case, we calculated the OCT A-line amplitude by taking the Hilbert transform of the simulated OCT signal and subsequently calculating the magnitude of the resulting complex signal. From both signals we determined the positions of the maximum signal gradients (the gradient of reflectivity profile is displayed in Figure 2-8) to localize the edges, and thus layer thickness. The results of are presented in Figure 2-9. Clearly, the incoherent point spread function recovers the correct layer thickness, i.e. 62.5 μm used in the simulation. However, it is the coherent PSF that is involved in OCT signal formation. Given the linear relation between recovered thickness and optical resolution found in this simulation, we propose that advanced segmentation algorithms may take this effect into account.

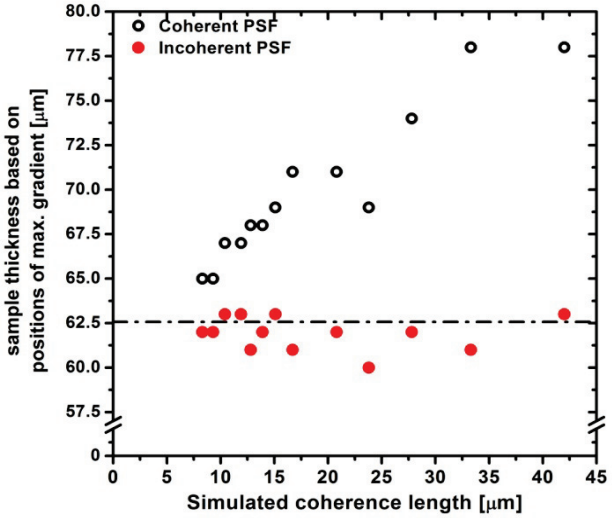


**Figure 2-9**: Simulated sample thickness for the coherent and incoherent point spread function displayed versus simulated coherence length. Dashed line shows input thickness.

In addition, speckle noise can in principle be a source of error, however, we used the average thickness of a circular A-scan around the fixation target and the influence of speckle noise cancels out. Moreover, in a previous study (21), using a Zeiss Stratus OCT system, it was shown that the signal strength or image quality influences the calculation of the RNFL thickness. Thickness was found to decrease when the signal strength was decreased. In our study we kept the image quality at a maximized level for all measurements. Likely the most important factory setting influencing thickness measurements is the refractive index (22). Throughout this

paper we assumed a constant n=1.35 for all systems, which was confirmed by private conversations with representatives of the different brands used in this study.

To fully elucidate the different responses of these systems requires the construction of multiple retina phantoms with varying (top) layer thicknesses. Such a study is beyond the scope of our present work and will be undertaken in the future. We note, however, that variations in layer thickness measurements within a single device much larger than the optical resolution are unlikely to occur in normally functioning, certified devices.

Leite *et al* (6) assessed the agreement of RNFL measurements among single devices of three SD-OCT brands. Similar to our findings, they showed an equal average thickness between Cirrus and Spectralis but higher thickness measured with an RTVue system.

## 2.5 CONCLUSION

To quantitatively compare RNFL thickness measurements between four brands of commercially available OCT systems, we developed a phantom that mimics the layered anatomy of the retina and provides high scattering contrast. The top layer (49 μm thickness) provides a constant RNFL-like "stimulus" to all OCT systems.

Statistically significant differences in thickness measurement between devices of one brand, and between brands were found. The clinical significance of these differences (maximum 3.6 μm within and maximum 7.7 μm between brands) is however difficult to determine. All systems overestimate the top layer thickness by 13 – 23 μm. To adequately explain this difference, knowledge on the implementation of the manufacturers' proprietary segmentation algorithm is needed.

Comparison of thickness measurements by SD-OCT systems using device independent, reproducible samples that mimic the relevant tissue geometry and optical properties is highly preferable. The phantom eye model, described in this study, is a useful tool to quantitatively determine differences between devices.

## 2.6 REFERENCES


1. D. Huang, E. A. Swanson, C. P. Lin, J. S. Schuman, W. G. Stinson, W. Chang, M. R. Hee, T. Flotte, K. Gregory, C. A. Puliafito and J. G. Fujimoto, "Optical Coherence Tomography," Science 254(5035), 1178-1181 (1991)
2. R. G. Mirza, M. W. Johnson and L. M. Jampol, "Optical coherence tomography use in evaluation of the vitreoretinal interface: A review," Surv. Ophthalmol. 52(4), 397-421 (2007)
3. M. E. J. van Velthoven, D. J. Faber, F. D. Verbraak, T. G. van Leeuwen and M. D. de Smet, "Recent developments in optical coherence tomography for imaging the retina," Prog. Retin. Eye Res. 26(1), 57-77 (2007)
4. R. Nguyen, D. Huang, M. R. Hee, T. PedutKloizman, J. G. Coker, J. R. Wilkins and J. S. Schuman, "Retinal nerve fiber layer distribution as measured by optical coherence tomography," Invest. Ophthalmol. Vis. Sci. 37(3), 5041-5041 (1996)
5. D. L. Budenz, R. T. Chang, X. R. Huang, R. W. Knighton and J. M. Tielsch, "Reproducibility of retinal nerve fiber thickness measurements using the stratus OCT in normal and glaucomatous eyes," Invest. Ophthalmol. Vis. Sci. 46(7), 2440-2443 (2005)
6. M. T. Leite, H. L. Rao, R. N. Weinreb, L. M. Zangwill, C. Bowd, P. A. Sample, A. Tafreshi and F. A. Medeiros, "Agreement Among Spectral-Domain Optical Coherence Tomography Instruments for Assessing Retinal Nerve Fiber Layer Thickness," Am. J. Ophthalmol. 151(1), 85-92 (2011)
7. M. N. Menke, P. Knecht, V. Sturm, S. Dabov and J. Funk, "Reproducibility of Nerve Fiber Layer Thickness Measurements Using 3D Fourier-Domain OCT," Invest. Ophthalmol. Vis. Sci. 49(12), 5386-5391 (2008)
8. A. O. Gonzalez-Garcia, G. Vizzeri, C. Bowd, F. A. Medeiros, L. M. Zangwill and R. N. Weinreb, "Reproducibility of RTVue Retinal Nerve Fiber Layer Thickness and Optic Disc Measurements and Agreement with Stratus Optical Coherence Tomography Measurements," Am. J. Ophthalmol. 147(6), 1067-1074 (2009)
9. J. S. Kim, H. Ishikawa, K. R. Sung, J. Xu, G. Wollstein, R. A. Bilonick, M. L. Gabriele, L. Kagemann, J. S. Duker, J. G. Fujimoto and J. S. Schuman, "Retinal nerve fibre layer thickness measurement reproducibility improved with spectral domain optical coherence tomography," Br. J. Ophthalmol. 93(8), 1057-1063 (2009)
10. N. Serbecic, S. C. Beutelspacher, F. Aboul-Enein, K. Kircher, A. reitner and U. schmidt-Erfurt, "Reproducibility of high resolution optical coherence tomography measurements of the nerve fiber layer with the new Heidelberg Spectralis optical coherence tomography," Br. J. Ophthalmol. 95(6), 804-810 (2010)
11. G. Savini, M. Carbonelli and P. Barboni, "Retinal Nerve Fiber Layer Thickness Measurement by Fourier-domain Optical Coherence Tomography: A Comparison Between Cirrus-HD OCT and RTVue in Healthy Eyes," J. Glaucoma 19(6), 369-372 (2010)
12. D. M. de Bruin, R. H. Bremmer, V. M. Kodach, R. de Kinkelder, J. van Marle, T. G. van Leeuwen and D. J. Faber, "Optical phantoms of varying geometry based on thin building blocks with controlled optical properties," J. Biomed. Opt 15(2), (2010)
13. D. J. Faber, F. J. van der Meer and M. C. G. Aalders, "Quantitative measurement of attenuation coefficients of weakly scattering media using optical coherence tomography," Opt. Express 12(19), 4353-4365 (2004)

14. T. G. van Leeuwen, D. J. Faber and M. C. Aalders, "Measurement of the axial point spread function in scattering media using single-mode fiber-based optical coherence tomography," Ieee Journal of Selected Topics in Quantum Electronics 9(2), 227-233 (2003)
15. T. S. Rowe and R. J. Zawadzki, "New developments in eye models with retina tissue phantoms for ophthalmic optical coherence tomography," J. N. Robert and L. C. Gerard, Eds., p. 822913, SPIE (2012).
16. D. J. Mordant, I. Al-Abboud, G. Muyo, A. Gorman, A. Sallam, P. Rodmell, J. Crowe, S. Morgan, P. Ritchie, A. R. Harvey and A. I. McNaught, "Validation of Human Whole Blood Oximetry, Using a Hyperspectral Fundus Camera with a Model Eye," Invest. Ophthalmol. Vis. Sci. 52(5), 2851-2859 (2011)
17. P. Lemaillet and J. C. Ramella-Roman, "Dynamic eye phantom for retinal oximetry measurements," J. Biomed. Opt 14(6), (2009)
18. F. Romero-Borja, K. Venkateswaran, A. Roorda and T. Hebert, "Optical slicing of human retinal tissue in vivo with the adaptive optics scanning laser ophthalmoscope," Applied Optics 44(19), 4032-4040 (2005)
19. D. J. Faber and T. G. van Leeuwen, "Doppler calibration method for Spectral Domain OCT spectrometers," J Biophoton. 2(6-7), 407-415 (2009)
20. J. M. Schmitt, S. H. Xiang and K. M. Yung, "Speckle in optical coherence tomography," J. Biomed. Opt 4(1), 95-105 (1999)
21. C. Y. L. Cheung, C. K. S. Leung, D. S. Lin, C. P. Pang and D. S. C. Lam, "Relationship between retinal nerve fiber layer measurement and signal strength in optical coherence tomography," Ophthalmology 115(8), 1347-1351 (2008)
22. G. J. Tearney, M. E. Brezinski, J. F. Southern, B. E. Bouma, M. R. Hee and J. G. Fujimoto, "Determination of the Refractive-Index of Highly Scattering Human Tissue by Optical Coherence Tomography," Opt. Lett. 20(21), 2258-2260 (1995)